

Possibility of a new level of space debris identification and tracking by Microwave Kinetic Inductance Detectors (MKIDs)

Saeed Vahedikamal⁽¹⁾, Ian Hepburn⁽²⁾,

⁽¹⁾ Mullard Space Science Laboratory, Department of Space and Climate Physics, UCL, Dorking, Surrey RH5 6NT, United Kingdom, Email: saeed.vahedikamal.11@ucl.ac.uk

⁽²⁾ Mullard Space Science Laboratory, Department of Space and Climate Physics, UCL, Dorking, Surrey RH5 6NT, United Kingdom, Email: i.hepburn@ucl.ac.uk

ABSTRACT

Microwave Kinetic Inductance Detectors (MKIDs) are considered as the most powerful detectors (on the pixel-by-pixel basis) [1]. MKIDs provide spectrally resolving single photon detectivity over the UV-Optical and Near IR wavelengths. We present an initial investigation into the potential detectability, based on the number of reflected and detected photons, of space debris via an MKID. The simulation results presented here are based on the initial models for space debris signal in an ideal situation. The results suggest the possibility of detecting objects of sub-millimetre sizes in LEO (Low Earth Orbit) ranges and object of sub-centimetre sizes in GEO (Geostationary Orbit) ranges.

1 Introduction

The ultimate in detection of light is by those detectors capable of detecting a single photon. Approximately 10^{18} photons per second per square metre per nanometre are incident on the Earth from sun light over the visible spectrum. Objects in orbit are visible by reflecting these photons. A detector capable of detecting single photons offers the ultimate in sensitivity.

Detectors developed to detect single photons have the additional benefit of being spectrally resolving and the ability to time tag individual photons. The goal of the last 20 years has been the steady increase in spectral resolution, increasing the number of pixels and the readout electronics. This has culminated in the development of the Microwave Kinetic Inductance Detector (MKID) [2]. All the developed single photon detectors have a common requirement in that to be able to detect the energy of a photon the detector must be cold. Typical this is in the region of 0.05 to 0.3 degrees Kelvin and are thus commonly labelled as cryogenic detectors. The uptake of cryogenic detectors has primarily been hindered not by the cryogenics but by the requirement to have an amplifier chain per detector or pixel in a detector array making large arrays unfeasible. An MKID pixel comprises a tuned LCR (inductance, capacitance, and resistance) resonance circuit. Each pixel can have its own unique resonance thus allowing large numbers of pixels to be readout by one feed line and a multichannel

frequency analyser. See [3] for a more detailed description.

At the Mullard Space Science Laboratory, University College London we have started investigating whether an array of MKIDs offers new imaging capability for space debris. In this paper we report on our initial investigation as to the number of photons that could be detected at the earth from various sizes and distances for space debris. At the present time we have considered only an idealized situation with realistic effects still to be included (e.g., sky background, airmass, spectral reflectance of debris material etc). As the project progresses limiting factors like sky photon background, atmospheric attenuation and the spectral reflectivity of materials commonly making up the space debris will be included.

2 MODELLING THE MKID RESPONSE

An MKID is a tuned inductor-capacitor-resistance (LCR) resonant circuit in which the inductor is superconducting. The detection principle is based on measuring the changes on the surface impedance of the superconducting inductor through the kinetic inductance effect, the resulting change in the inductance changes the resonant frequency which is detected. The MKID is sensitive enough to detect individual photons.

We have derived the MKID response to incident photons as a Probability Density Function (PDF) of the output signal based on the wavelength dependant energy resolution such as the one shown in the Figure 1-a. The PDF is applied to the incident signal creating a signal as detected by the MKID, this is shown in Figure 1-b for three narrow band laser lines. Figure 1-c shows the measured MKID output when illuminated with a laser set to those three wavelengths. The spectral resolution is defined as:

$$R_0 = \frac{\lambda_0}{FWHM} \quad (1)$$

Where FWHM is the full width half maximum of the output signal and λ_0 is the peak wavelength of the detected photons.

The output signal from MKIDs can be described as a Gaussian (normal) distribution of the arrival photons

(received energies) around the peak of the signal. Then, the relationship between FWHM and the standard deviation of a signal with a peak at λ_0 is

$$\sigma_0 = \frac{FWHM}{2\sqrt{2 \ln(2)}} = \frac{1}{2\sqrt{2 \ln(2)}} \left(\frac{\lambda_0}{R_0} \right) \quad (2)$$

Also, the MKIDs response to a stream of photons with the wavelength of λ_0 can be defined as a Probability Density Function (PDF) for a normal distribution of photons (energies) around the signal peak, which is

$$f(\lambda|\lambda_0, \sigma_0) = \frac{1}{\sigma_0 \sqrt{2\pi}} e^{-0.5 \left(\frac{\lambda - \lambda_0}{\sigma_0} \right)^2} \quad (3)$$

$f(\lambda|\lambda_0, \sigma_0)$ gives the distribution of photons (energies) around a peak at λ_0 which can be interpreted as the likelihood of detecting photons with different wavelengths (different level of energies) while collecting photons of a specific wavelength (energy). Substituting the standard deviation by the resolution and further rearrange the equation, the Probability Density Function (PDF) for a normal distribution of photons (energies) can be also described in terms of the resolution, instead of the standard deviation.

$$\begin{aligned} f(\lambda|\lambda_0, R_0) & \quad (4) \\ &= 2 \left(\sqrt{\frac{\ln(2)}{\pi}} \right) \left(\frac{R_0}{\lambda_0} \right) \left(\frac{1}{4} \right) \left(\left(\frac{R_0}{\lambda_0} \right) \lambda - R_0 \right)^2 \end{aligned}$$

If the resolutions for MKIDs across a spectrum, with a range of wavelengths from λ_i to λ_n , are defined as R_i to R_n , then the MKIDs response for that spectrum can be generated by the sum of distribution of photons at each wavelength as follow

$$\{\lambda_i \leq \lambda \leq \lambda_n\}, \quad f(\lambda) = \sum_{\substack{\lambda_0=\lambda_i \\ \sigma_0=\sigma_i}}^{\substack{\lambda_0=\lambda_n \\ \sigma_0=\sigma_n}} f(\lambda|\lambda_0, \sigma_0) \quad (5)$$

The response function, $f(\lambda)$, describes the MKIDs response to a defined spectrum for $\lambda_i \leq \lambda \leq \lambda_n$, in terms of a Probability Density Function. If the number of photons in each wavelength of the measured (arrival) signal is defined by

$$N(\lambda) = \sum_{\lambda_0=\lambda_i}^{\lambda_0=\lambda_n} N(\lambda_0) \quad (6)$$

then the MKIDs will output will be

$$I_N(\lambda) = \sum_{\substack{R_0=R_n \\ \lambda_0=\lambda_n \\ \lambda_0=\lambda_i \\ R_0=R_i}} f(\lambda|\lambda_0, \sigma_0) \cdot N(\lambda_0) \quad (7)$$

Where, $I_N(\lambda)$ is the intensity of the output signal in terms the photon counts for each wavelength.

Assuming $N(\lambda_0)$ in Figure 1-c. consists of 400,000 photons at 808 nm peak, 200,000 at 980 nm peak and 150,000 photons at 1310 nm peak. Then, based on Eq. 7 the MKID output signal can be reconstructed as the histogram shown in Figure 1-b.

The similarity of Figure 1-b and Figure 1-c. verifies the reliability and accuracy of this method for simulating the MKIDs output.

Similarly, if the arrival signal is based on the energy received at each wavelength and expressed as

$$E(\lambda) = \sum_{\lambda_0=\lambda_i}^{\lambda_0=\lambda_n} E(\lambda_0) \quad (8)$$

Then the MKIDs output for that signal can be expressed in terms of energy by

$$I_E(\lambda) = \sum_{\substack{R_0=R_n \\ \lambda_0=\lambda_n \\ \lambda_0=\lambda_i \\ R_0=R_i}} f(\lambda|\lambda_0, \sigma_0) \cdot E(\lambda_0) \quad (9)$$

Therefore, Eq. 7 and Eq. 9 can be used for simulating the MKIDs response to a received signal/light in terms of either energy or photon counts.

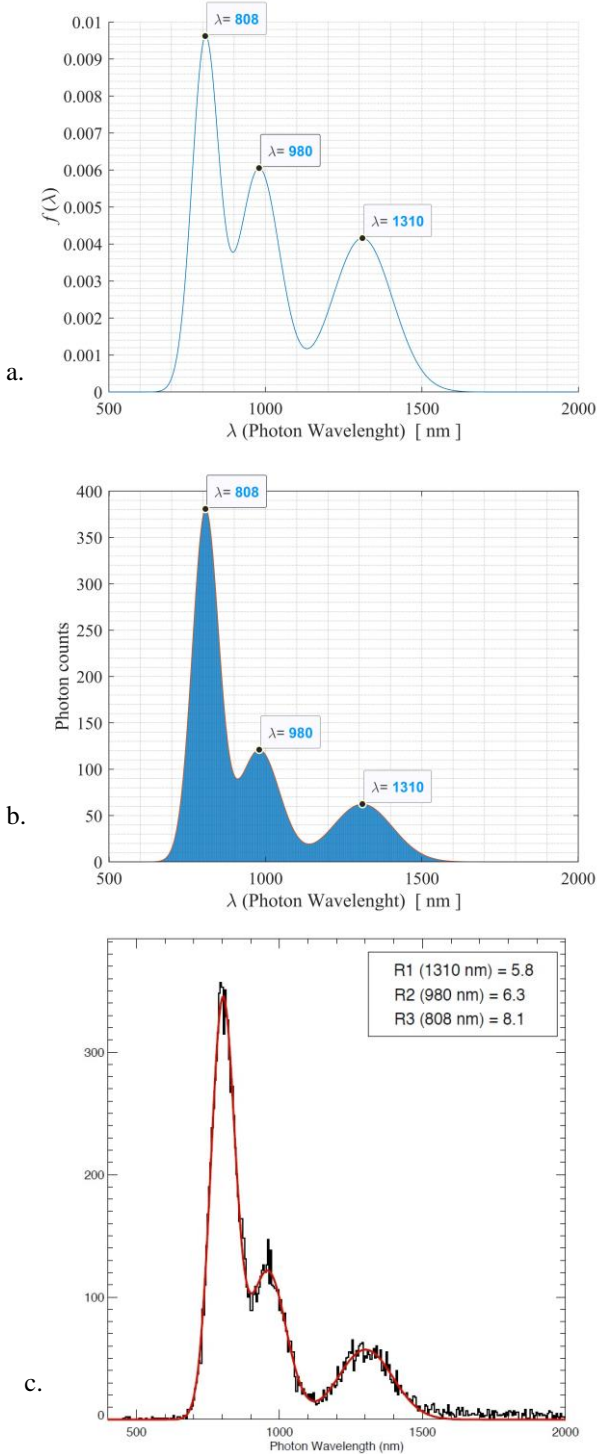


Figure 1. a: The combined MKID response as the Probability Density Function (PDF) for the wavelengths of 1310 nm, 980 nm, and 808 nm. b: Reconstruction of the MKID response, for the wavelengths of 1310, 980, and 808 nm laser light, using their corresponding resolutions. c: The histogram of photon wavelengths measured by an MKID while illuminated with 1310, 980, and 808 nm laser light [4]. The inset shows the MKID resolutions for three wavelengths.

The resolution of the detector is a crucial component in the system as it defines the detection capabilities and the detail in the output signal. The quest for developing MKIDs with improved response and characteristics is an on-going process. Table 1 presents the MKIDs resolution values based on the results from a recent study, which demonstrates significant improvement in their dynamic range, for multiple wavelengths ranging from 406 nm to 1310 nm [5].

Table 1. The resolution numbers achieved for a hafnium optical to near-IR MKID in different conditions in a recent study [5].

Wavelength [nm]	R (Resolution)
406	17
663	13
814	12
917	12
979	12
1110	10
1310	9.6

Using the data in Table 1 and assuming a detector collects only photons of peak wavelengths at 406 nm, 663 nm, 814 nm, 917 nm, 979 nm, 1110 nm, and 1310 nm with a flux equivalent to sunlight incident on the Earth, the spectral output of the MKID will be as shown in Figure 2.

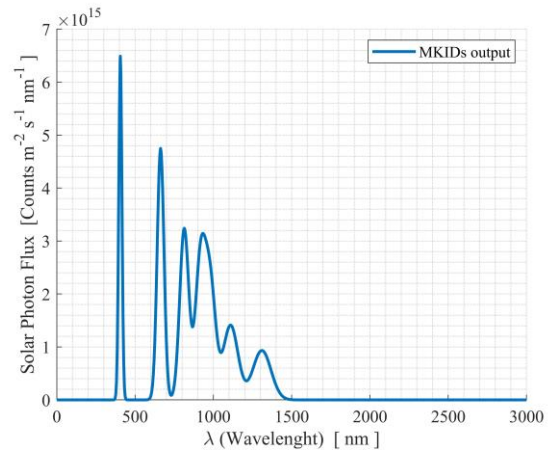


Figure 2. The expected MKIDs output if receive the photons from sunlight at wavelengths of 406 nm, 663 nm, 814 nm, 917 nm, 979 nm, 1110 nm, and 1310 nm.

The available experimental data, for the MKIDs resolution, from actual measurements, offers limited number of values across the spectrum. Hence an extrapolation of the current experimental data is necessary for simulating the MKIDs response within a

wider range of wavelength in the spectrum. Here, we use the values provided in Table 1 as the main reference points for estimating the resolution across the spectrum. The resolution is expected to increase for the shorter wavelengths (photons with higher energies). However, we have assumed that the highest value for the resolution is 17 and it will remain the same for photons with wavelengths less than 406 nm. We expect an almost linear drop in the resolution for the IR region and wavelengths longer than 1310 nm [6]. It must be mentioned that the main problem for the detection in longer wavelengths (lower energies) is while reaching the wavelengths of 1500-1600 nm and going beyond, the 300 K° thermal blackbody starts adding to the background noise. This, in effect, limits the detection range to the near-IR region of the spectrum. A possible solution for this problem maybe via options such as a cryogenic telescope (i.e. cooled optics), spreading sky background over more pixels or operation in space.

In order to have a near continuous function for the MKID spectral resolution in order to simulate a complete spectrum we have divided the spectral resolution into six separate regions as presented in Table 2. Region 1 contains the wavelengths from 0.5 nm up to 406 nm. As stated above, the presumption is that the resolution hits its maximum value of 17 at the wavelength of 406 nm and remain at this value for the shorter wavelengths down to 0.5 nm. Also, the resolution stays at a constant value of 12 throughout region 4. A further assumption is that the resolution reduces linearly for wavelengths longer than 1110 nm, reaching a value of 9.6 for 1310 nm and goes to zero at 6110 nm.

Table 2. The MKIDs resolution for different regions in the spectrum, calculated based on the most recent available data.

Region	Section of the spectrum	MKIDs resolution
1	$0.5 \text{ nm} \leq \lambda \leq 406 \text{ nm}$	$R = 17$
2	$406 \text{ nm} < \lambda \leq 663 \text{ nm}$	$R = -0.0156 \lambda + 23.319$
3	$663 \text{ nm} < \lambda < 814 \text{ nm}$	$R = -0.0066 \lambda + 17.391$
4	$814 \text{ nm} < \lambda \leq 917 \text{ nm}$	$R = 12$
5	$979 \text{ nm} < \lambda \leq 1110 \text{ nm}$	$R = -0.0153 \lambda + 26.947$
6	$1110 \text{ nm} < \lambda$ up to near-IR	$R = -0.002 \lambda + 12.22$

Figure 3 shows the variations of the MKIDs resolution, based on Table 2,. Using these values for resolution and applying them to the solar spectrum, based on Eq. 9, we can generate the MKIDs response to the solar Spectrum as shown in Figure 4. The reference solar irradiance spectrum has been taken from SOLAR-ISS spectrum, Version: 1.1 (Date: 18-October-2017) which is from solar observations performed by the SOLAR/SOLSPEC

space-based instrument [7].

As can be seen in Figure 4 the simulated output signal of MKIDs misses some of the detail in the solar spectrum and appears softer compared to the high-resolution solar spectra., This is due to the much lower spectral resolution of the MKID which results in spreading the signal for each wavelength across to other wavelengths. Although this causes a partial loss of the information, on the other hand, it can help to increase the intensity of the signal in the areas with deeper spectral lines where there is smaller number of photons (less energies) in the sunlight. Therefore, losing the spectral lines in the output signal acts as binning the data and might increase the chance of detecting the signal in some cases.

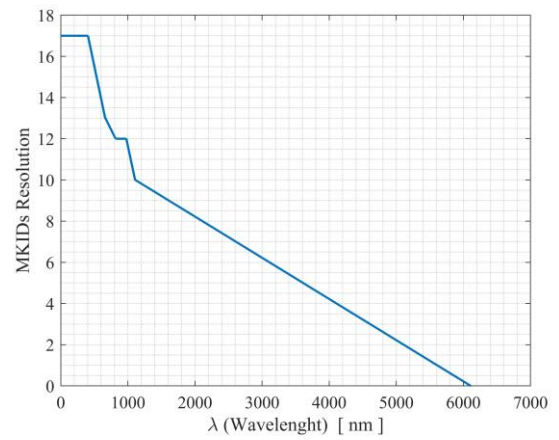


Figure 3. Presumed values for the MKIDs resolution at different wavelengths across the spectrum.

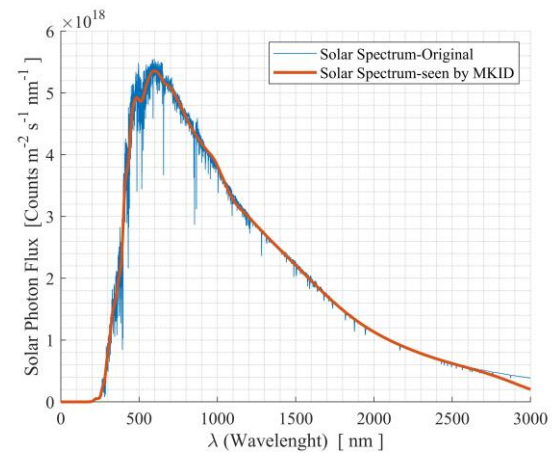


Figure 4. MKIDs response to the solar spectrum in terms of photon flux for each nanometre of the spectrum.

3 Defining and modelling an idealised signal from an object in orbit

In normal conditions, space debris do not reach high enough temperatures to emit visible light and only emit light within the infrared (IR) range of the spectrum. The thermal IR signatures from space debris, particularly the ones of small sizes (objects with less than 10 cm in diameter) are extremely weak to be detected by detection instruments on the Earth. On the other hand, all objects in the orbit can receive a similar intensity of Sun light to that on the earth. Therefore, the illuminated light from space debris is mainly their surface reflection of Sun light.

There are many factors that can affect the intensity and the nature of the reflected sunlight from the surface of the objects in orbit and received by a ground-based detector. Two of the main factors are the size and distance of the object. In our initial analysis presented here, these two factors are used to produce a simplified model for the signal. Also, for simplicity the ideal object is considered to have a flat and circular shape with 100% reflectivity. The effect of the surface, shape and reflectivity of the object will be added to the model along with the other elements that can affect the signal in the next phase of the model's development.

The intensity of the received signal can be defined as

$$I_s = I_* f(d_o, r_o, \theta_o) \cdot F_a \quad (10)$$

Where,

I_* is the intensity of the sunlight as it hits the object.

$f(d_o, r_o, \theta_o)$ is a function based on the object distance, object radius and angle of the object towards the sunlight, describing the effect on the intensity of the signal.

F_a is the attenuation factor which is a combination of all the other elements that might affect the signal. This is considered as 1 in the initial analysis presented here.

To derive the $f(d_o, r_o, \theta_o)$, we consider the scenario shown in Figure 5. In this scenario the sunlight hits an object in orbit that is facing the Sun at an angle of θ_o . For objects with an altitude up to GEOs (geostationary orbits), the distance of an object to the Sun can be estimated to 1 AU (Astronomical Unit), which is the Sun to Earth distance. The size of the object next to the Sun appears as a very small point, so the reflected sunlight from the object will expand with an angle similar to the Sun's apparent angle.

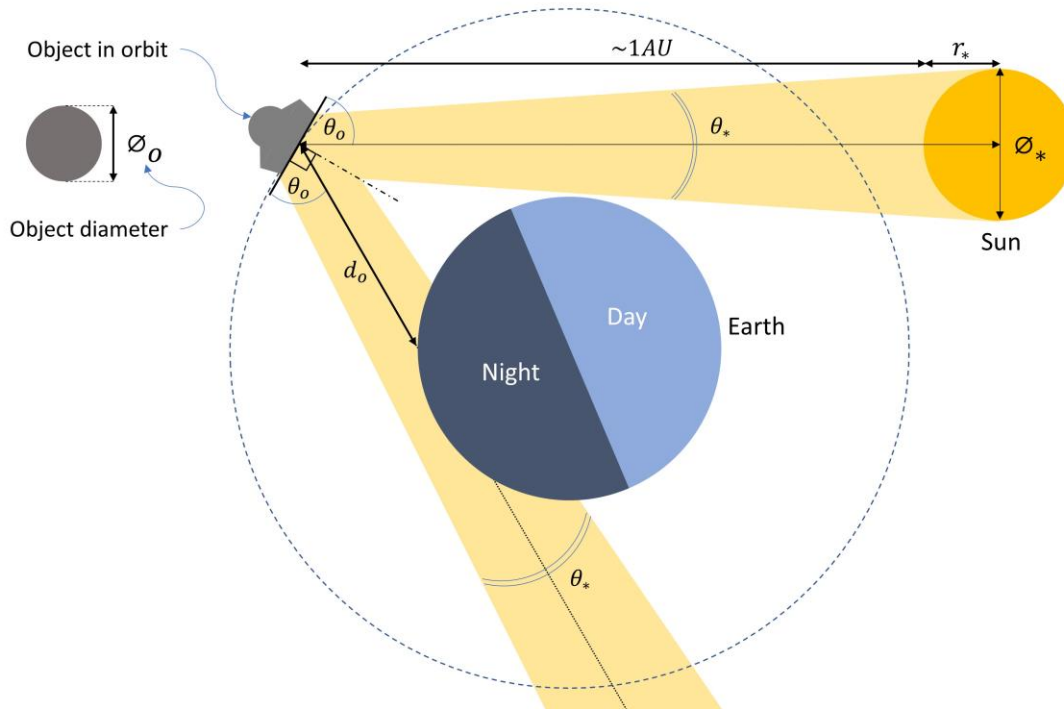


Figure 5. The reflected sunlight from an object in the Earth's orbit expand with an angle of θ_* as it approaches the detector on the ground. The size of the object is exaggerated and, in reality, it is equivalent to a point of reflection.

The apparent angle of the Sun can be calculated as

$$\theta_* = \tan^{-1} \frac{R_*}{1AU + R_*} \quad (11)$$

Where the R_* is the radius of the Sun and $1AU$ is the distance from the Sun to the Earth.

For an ideal object with a circular surface, the effective surface area that reflects the light is

$$A_o = \pi(r_o \sin \theta_o)^2 \quad (12)$$

Where, r_o is the radius of the object and θ_o is the angle of the object towards the Sun.

Also, the area that is covered by the arrival signal is

$$A_s = \pi r_s^2 \quad (13)$$

Where, the r_s is the radius covered by the signal as it is incident on the detector.

The signal expands by the angle of θ_* , as it moves away from the object, so the radius covered by the signal can be derived as

$$r_s = r_o \sin \theta_o + d \tan \left(\frac{\theta_*}{2} \right) \quad (14)$$

Where, r_o is the radius, and d_o is the distance of the object.

Also, the relation between the intensity of the signal (I_s) and the intensity of the reflected sunlight (I_o) adjacent to the object is

$$I_s A_s = I_o A_o \cdot F_a \quad (15)$$

By substituting the values for A_s and A_o we can show

$$I_s \pi r_s^2 = I_o \pi (r_o \sin \theta_o)^2 F_a$$

$$I_s \left[r_o \sin \theta_o + d_o \tan \left(\frac{\theta_*}{2} \right) \right]^2 = I_o (r_o \sin \theta_o)^2 \cdot F_a$$

Therefore, the function describing the effect of the distance and size of the object can be expressed as

$$f(d_o, r_o, \theta_o) = \left[\frac{r_o \sin \theta_o}{r_o \sin \theta_o + d_o \tan \left(\frac{\theta_*}{2} \right)} \right]^2 \quad (16)$$

Combining (eq. 4.2) & (eq. 4.1) gives

$$I_s(d_o, r_o, \theta_o) = I_* \left[\frac{r_o \sin \theta_o}{r_o \sin \theta_o + d_o \tan \left(\frac{\theta_*}{2} \right)} \right]^2 F_a \quad (17)$$

which describes the intensity of the arrival signal based on the object distance, object radius and angle of the object towards the sunlight.

4 SIMULATION RESULTS

The simulation results presented below represent an idealized condition in which F_a has been set to 1 in Eq. 10. The debris has been considered as perfectly flat round objects with 100% reflectivity at all wavelengths and the light from an object to the detector is unattenuated. Therefore, the debris signal is influenced by only three factors, namely, θ_o (the angle of the object towards the Sun), r_o (the object radius/size), and d_o (the object distance to the detector).

Figure 5 shows that for an effective ground-based observation, θ_o must be between 45° and 90° . If θ_o is smaller than 45° then the observation needs to be performed during the daytime and, if θ_o is larger than 90° then the reflected light does not intercept the Earth. The angle θ_o determines the object's effective surface area that is exposed to the incoming sunlight; hence, it determines how much light can be reflected. Figure 6 shows the scenario of an object with a diameter of 10mm at a distance of 50000 km from the Earth and detector with various angles to the Sun. From Figure 6, it can be seen that the intensity of the photon flux is higher for wider angles.

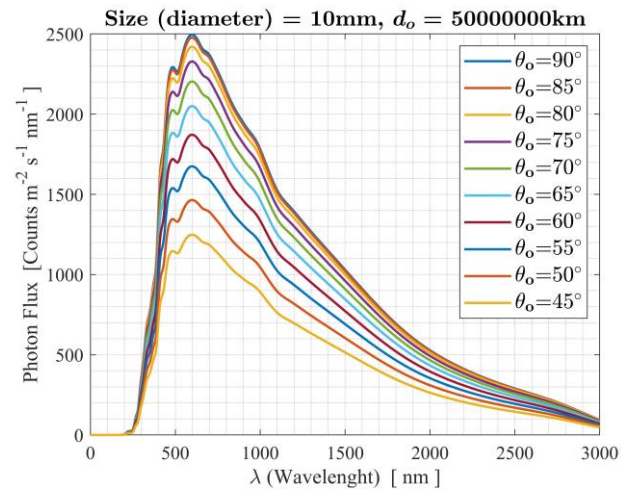


Figure 6. The MKID outputs, based on simulations, for detected light that is received from an object in orbit while facing the Sun at different angles.

It is important to remember that the angle θ_o also,

determines the observation angle as well as the location of the observation. This means, that for any given set up, the detector can collect light only from objects with a certain θ_o . In order to condense our results, we have chosen to present data for an obituary angle of 70° . However, Figure 7 shows the effect of θ_o on the intensity of the received light and will thus enable scaling of our presented results for other angles.

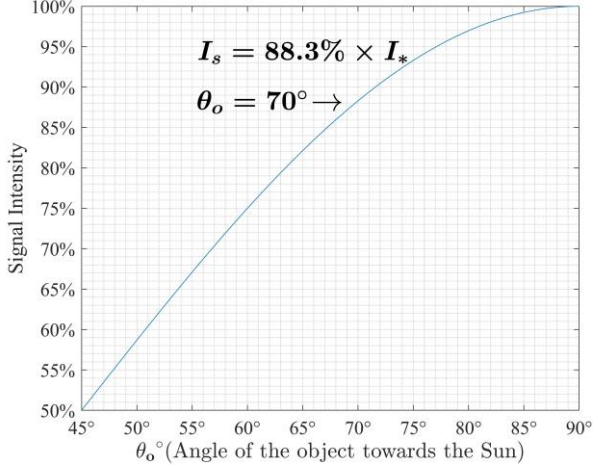


Figure 7. The blue line shows the percentage of the reflected sunlight by an object based on its orientation towards the Sun.

The simulated MKID spectra show that the peak of the signal occurs at a wavelength of 600 nm. Figure 8 shows the variation of photon flux at the peak of the signal for objects of different sizes at multiple distances from the detector. From Figure 5, you can see the distance of the object to the detector is longer than its distance to the Earth (its altitude) for θ_o larger than 45° .

Also, the results demonstrate that the intensity of the signal has a direct relation with the square of the object size and inverse square of the object distance.

$$I_s \sim \frac{\phi_o^2}{d_o^2} \quad (18)$$

Where, ϕ_o is the diameter (size) of the object.

Here, we considered the criteria for an acceptable detection is to have an output signal with a minimum photon flux of $500 \text{ photons m}^{-2} \text{ s}^{-1} \text{ nm}^{-1}$ over the wavelength range of 470 nm to 750 nm. This range covers most of the visible light and small portion of infrared light.

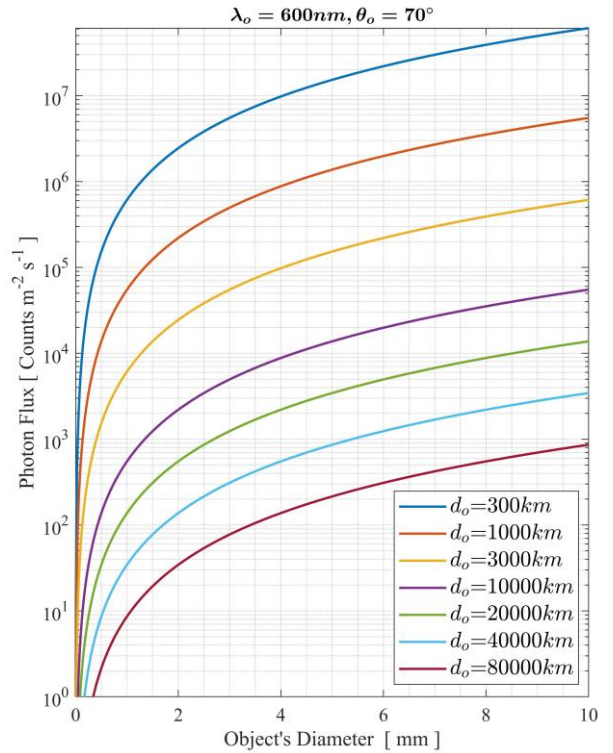
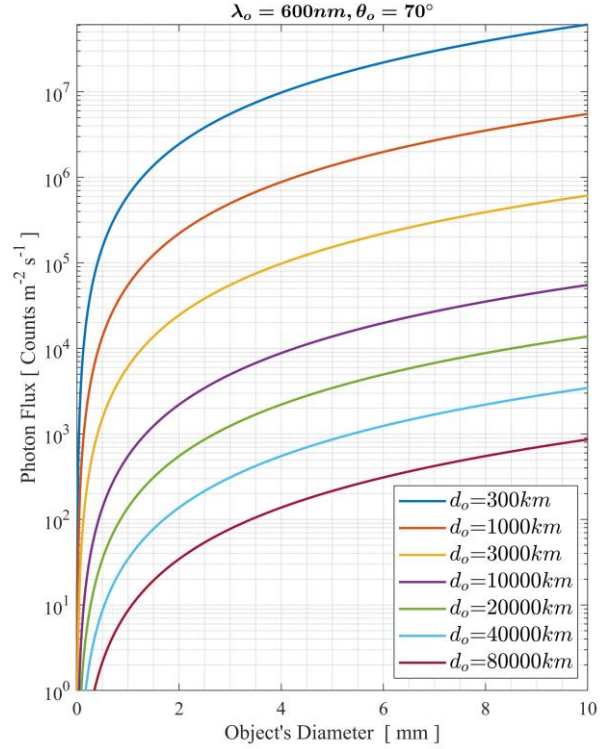


Figure 8. Simulations shows the MKID response to photons of 600 nm wavelength that are received from objects with sizes up to 10mm at different distances from the detector.

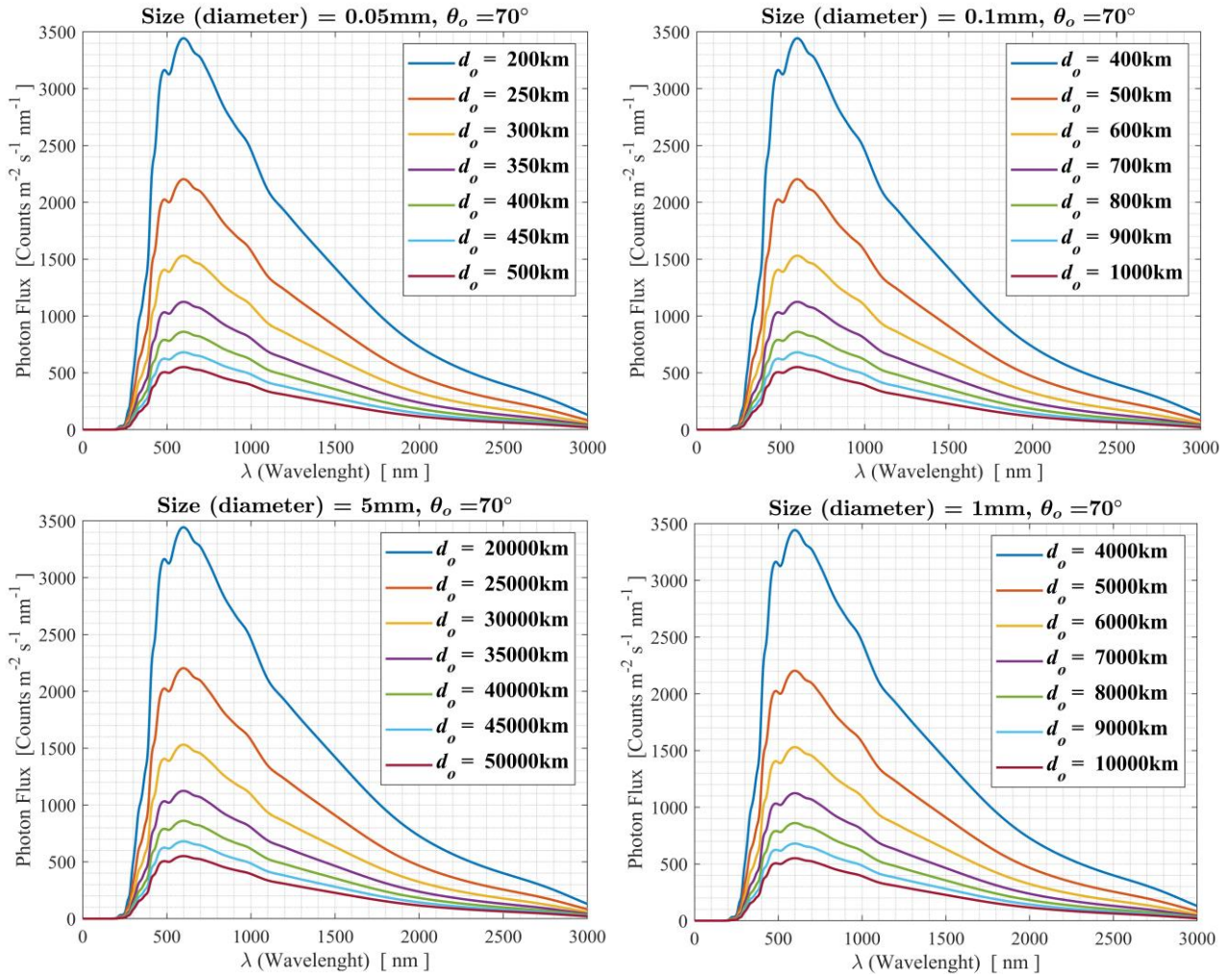


Figure 9. The MKID outputs, obtained from simulations, for three different objects of varying sizes at multiple distances from the detectors in 4 different orbit ranges.

Fig 9 shows that via this criteria reflected solar light from debris of 50 μm size at 500 km, 100 μm at 1000 km, 1mm at 10,000 km, and 5 mm at 50,000 km are all considered detectable while facing the Sun at an angle of 70°. Using any of these objects as a reference, it can be shown that the relation between the sizes/diameters (ϕ_o) and the distances (d_o) of the objects for effective observations under our criteria is

$$\phi(\text{mm}) \geq d_o(\text{km}) \times 10^{-4} \quad (\theta_o = 70^\circ) \quad (19)$$

Figure 10 illustrates Eq. 19 by a line which can be used as a detectability scale.

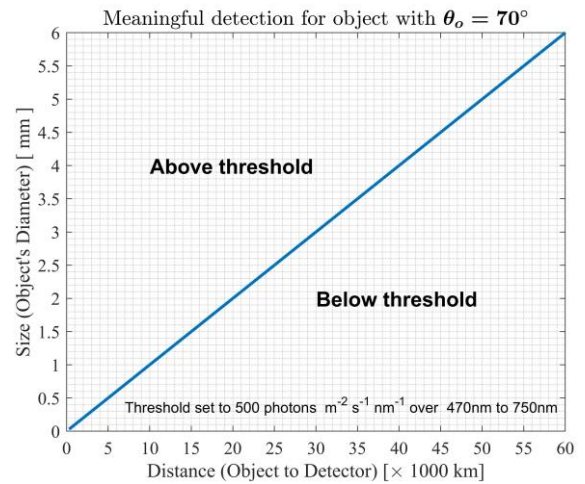


Figure 10. The region above the threshold defines the observable size of objects, based on our criteria and the corresponding distances to the detector. The blue line shows the minimum size for an effective detection.

5 Conclusion

In this work, we have presented our initial investigation into the use of single photon detection via MKIDs for detecting space debris. Our detection model so far is based on an idealised scenario which considers the influence of three properties of the debris (their distance to the detector, their sizes, and their angle towards the Sun) on the reflected sunlight from their surface. The results from initial simulations indicate the possibility of a valid detection for objects of sub-millimetre sizes in LEO ranges and sub-centimetre sizes in GEO ranges. Although, these are encouraging results, the other factors that can significantly attenuate the incoming light from debris or interfering with the observation should not be ignored. In the next stage of our study, the role of three further attenuating factors will be considered i.e., sky background¹, stellar background², and airmass³. The objects composition, shape & surface structure determine its reflectivity and the amount of light reflected towards the detector and thus must also be included in our continuation of this work. These additional elements can be added to F_a of Eq. 10. By including these further factors and adding more complexity to the model it is likely to result in a considerable drop in the detectable photons from debris. However, the initial results suggest detecting debris with sizes smaller than 10 cm even at high altitude ranges is not farfetched. Achieving such a capability would we suggest add significant value to current systems for detecting and tracking space debris.

6 Acknowledgements

Saeed Vahedikamal gratefully acknowledges the award of an STFC postgraduate studentship. The authors would also like to express their thanks to Prof B Mazin of UCSB for his advice on MKIDs.

7 References

- [1] B. A. Mazin, "KRAKENS: a general purpose MKID integral field spectrograph for the Keck I telescope," Austin, Texas, United States, 2018.
- [2] B. A. Mazin, *Microwave Kinetic Inductance Detectors*, Pasadena, California: California Institute of Technology, 2004.
- [3] A. B. Walter, *MEC: The MKID Exoplanet Camera for High Speed Focal Plane Control at the Subaru Telescope*, Santa Barbara: University of California Santa Barbara, 2019.
- [4] P. Szypryt, S. R. Meeker, G. Coiffard, N. Fruitwala, B. Bumble, G. Ulbricht, A. B. Walter, M. Daal, C. Bockstiegel, G. Collura, N. Zobrist, I. Lipartito and B. A. Mazin, "Large-format platinum silicide microwave kinetic inductance detectors for optical to near-IR astronomy," *Optics Express*, vol. 25, no. 21, pp. 25894-25909, 2017.
- [5] N. Zobrist, N. Klimovich, B. H. Eom, G. Coiffard, M. Daal, N. Swimmer, S. Steiger, B. Bumble, H. G. LeDuc, P. Day and B. A. Mazin, "Improving the dynamic range of single photon counting kinetic inductance detectors," *Journal of Astronomical Telescopes, Instruments, and Systems*, vol. 7, no. 1, p. 010501, Jan. 20, 2021.
- [6] B. Mazin, *Private Communication*, 2020.
- [7] M. Meftah, L. Damé, D. Bolsée, A. Hauchecorne, N. Pereira, D. Sluse, G. Cessateur, A. Irbah, J. Bureau, M. Weber, K. Bramstedt, T. Hilbig, R. Thiéblemont, M. Marchand, F. Lefèvre, A. Sarkissian and S. Bekki, "SOLAR-ISS: A new reference spectrum based on SOLAR/SOLSPEC observations," *A&A (Astronomy & Astrophysics)*, vol. 661, p. A1, 2018.

¹ The amount of light (number of photons) received in the unit area (m^2) which is produced by the scattering effect in the atmosphere.

² The amount of light (number of photons) received in the

unit area (m^2) from the other celestial objects.

³ The attenuation of the signal caused by absorption of light as it passes through the atmosphere. This can be described quantitatively by the Beer-Lambert law.